Recognition of Planar and Nonplanar Ligands in the Malachite Green – RNA Aptamer Complex

Jeremy Flinders,[a] Steven C. DeFina,[a] David M. Brackett,[a] Chris Baugh,[b] Charles Wilson,[c] and Thorsten Dieckmann*[a]

Ribonucleic acids are an attractive drug target owing to their central role in many pathological processes. Notwithstanding this potential, RNA has only rarely been successfully targeted with novel drugs. The difficulty of targeting RNA is at least in part due to the unusual mode of binding found in most small-molecule – RNA complexes: the ligand binding pocket of the RNA is largely unstructured in the absence of ligand and forms a defined structure only with the ligand acting as scaffold for folding. Moreover, electrostatic interactions between RNA and ligand can also induce significant changes in the ligand structure due to the polyanionic nature of the RNA. Aptamers are ideal model systems to study these kinds of interactions owing to their small size and the ease with which they can be evolved to recognize a large variety of different ligands. Here we present the solution structure of an RNA aptamer that binds triphenyl dyes in complex with malachite green and compare it with a previously determined crystal structure of a complex formed with tetramethylrosamine. The structures illustrate how the same RNA binding pocket can adapt to accommodate both planar and nonplanar ligands. Binding studies with single- and double-substitution mutant aptamers are used to correlate three-dimensional structure with complex stability. The two RNA – ligand complex structures allow a discussion of structural changes that have been observed in the ligand in the context of the overall complex structure. Base pairing and stacking interactions within the RNA fold the phosphate backbone into a structure that results in an asymmetric charge distribution within the binding pocket that forces the ligand to adapt through a redistribution of the positive partial charge.

Introduction

RNA plays a central role in many biological processes and thus represents an attractive target for drug development. Despite this potential, only a few drugs that target RNA are in use or development.[1–5] One of the main roadblocks on the way towards rational structure-based design of ligands and drugs that target RNA is the mode of recognition found in most complexes between RNA and small molecules. Ligand recognition and binding is achieved in a very different manner from most proteins: the ligand acts as a scaffold for folding the RNA into an intricate three-dimensional structure and becomes an integral part of the structure. This mode of recognition has been termed "ligand-induced folding" or "adaptive binding"[6–8] and has been observed in most small-molecule-binding RNAs characterized to date. For example, the structure of the ATP-binding RNA aptamer illustrated that the ligand is recognized through a network of hydrogen bonds and stacking interactions.[9, 10] The binding pocket of the free RNA is very dynamic and largely unfolded, and converts into a well-defined structure only in the presence of ATP or AMP. In addition to the structural changes in the RNA, it has recently been shown that the ligand can also undergo significant changes with respect to its conformation and charge distribution upon binding to RNA.[11]

Aptamers are RNA or DNA molecules which are selected in vitro to bind ligand molecules with high specificity and affinity.[12, 13] A great variety of these sequences have been identified to date (see refs. [14 – 16] for reviews) and several structures have been determined by NMR spectroscopy or X-ray crystallography.[9, 10, 17–26] Aptamers are of great interest because they mimic recently discovered riboswitches that control gene expression[27–29] and are of use as molecular tools in several areas of chemistry and medicine.[30–35] Furthermore, as a result of their generally small size they are ideal model systems to study complex formation, RNA folding, and structure by means of NMR spectroscopy and crystallography. Many applications make use of the adaptive binding and the resulting changes in structure and dynamics of the RNA. For example, incorporation of an aptamer sequence into a particular RNA sequence can enable the molecule to recognize a specific protein[36, 37] or act as a

[a] *J. Flinders, S. C. DeFina, D. M. Brackett, Prof. T. Dieckmann*
Department of Chemistry
University of California
Davis, CA 95616 (USA)
Fax: (+1) 530-7528995
E-mail: dieckman@chem.ucdavis.edu

[b] *Dr. C. Baugh*
Anadys Pharmaceuticals
Department of Screening Sciences and Technologies
9050 Camino Santa Fe
San Diego, CA 92121 (USA)

[c] *Dr. C. Wilson*
Archemix
20 Hampden Street
Boston, MA 02119 (USA)

  DOI: 10.1002/cbic.200300701

ligand-dependent switch which can turn RNA function on and off.[38, 39] Adaptive binding also allows many aptamers to recognize derivatives of the original selection target. For example, the ATP-binding aptamer can bind NAD^+, 7-deazaadenosine, and 2′-*O*-methyl adenosine, albeit with reduced affinities.[6, 40] The removal of a single hydrogen bond between ligand and RNA in the ATP aptamer leads to K_D values that are reduced by two orders of magnitude relative to the original complex.[6] In general, a derivative of the original target molecule can bind to an aptamer with detectable affinity as long as the overall structure of the binding pocket remains similar and most of the stabilizing interactions between RNA and ligand are maintained.

In order to fully understand the molecular basis for folding around a ligand and to allow the rational design of new RNA ligands and drugs one needs to understand the energetic contributions of the molecular interactions that determine binding affinity and specificity. As a result of the polyanionic nature of RNA, electrostatic interactions play an important role in determining complex stability together with hydrogen bonds and base stacking interactions. We have chosen the malachite green (MG) binding aptamer as a model system to explore the role of these interactions. The aptamer was selected in vitro specifically to bind MG (Figure 1 A).[41] The molecule also binds

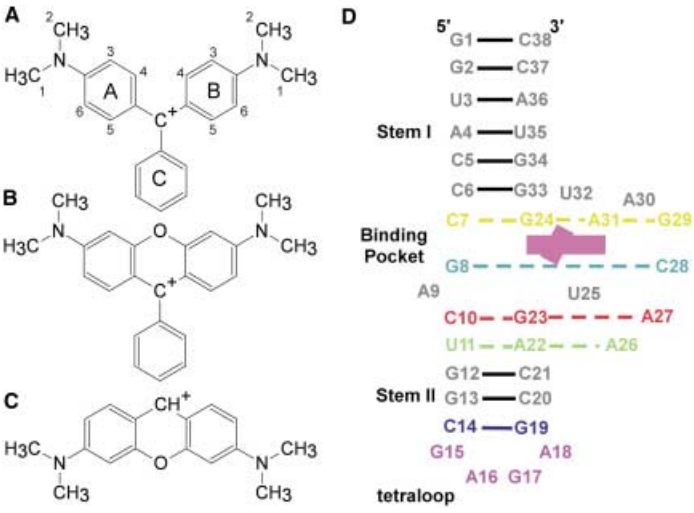

Figure 1. *Structures of malachite green (A), tetramethylrosamine (B), pyronin Y (C) and schematic of the crystal structure base stacking and secondary structure (D). The MG structure indicates the numbering scheme used for the protons. The color scheme of the aptamer sequence used in D is applied throughout this publication: yellow indicates the base quadruple, red and green mark the base triples, cyan the G8 – C28 base pair and purple the GNRA tetraloop. The base pair adjacent to the tetraloop is shown in dark blue, the other stem base pairs are colored grey.*

related organic dyes, such as tetramethylrosamine (TMR, Figure 1 B) and pyronin Y (PY, Figure 1 C), with K_D values in the 50 – 200 nM range. Crystal violet (CV), which differs from MG by just one additional *N*-dimethyl group, has no detectable binding to the aptamer. The three-dimensional structure in complex with TMR was determined by X-ray crystallography[24] (Figure 1 D). In the presence of TMR, the RNA folds rapidly to form a complex structure around the ligand with the dye stacked between a base quadruple (C7 · G24 · G29 · A31) and a Watson – Crick base pair (G8 · C28). The binding pocket is closed on one side by the aromatic rings of A9 and A30 which stack with each other and the unmodified phenyl ring of TMR. The MG aptamer is unique with respect to its mode of ligand recognition: the ligand and RNA interact only through base stacking of the nucleic acid with the aromatic rings of the dye and through electrostatic interactions. This feature makes the aptamer an excellent model system for studying the effects of stacking and electrostatic interactions that are masked by hydrogen bond effects in most systems. However, no crystals suitable for structure determination could be obtained for any complex but that with TMR. We initiated solution NMR studies of the aptamer in complex with its original selection target malachite green as a first step to investigate how different ligands are recognized and to explore potential differences between the structures in solution and the crystal. The crystal structure of the TMR – RNA complex was used to greatly streamline the NMR structure determination and limit the number of specifically and fully labeled samples needed. Herein we present the solution structure of the MG – RNA complex, compare it with the X-ray crystal structure of the TMR – RNA complex, and discuss the ability of the RNA to adapt to binding of different ligands.

Results

Design and synthesis of aptamer sequences for NMR studies

Initial NMR studies were performed by using an aptamer, with a sequence identical to the one used for X-ray studies (RNA1, Figure 1 D), and both MG and TMR dyes. Both complexes gave well-resolved NOESY spectra in 100% D_2O and 90% H_2O. However, the spectra of the MG – RNA complex have sharper lines under the NMR conditions used. The high symmetry of the first stem in RNA1 meant that obtaining assignments in this region was problematic; therefore, a second sequence was designed (RNA2) in which the U3 · A36 base pair was changed to a G · C pair and the GNRA tetraloop was replaced by a UUCG tetraloop. This sequence was used to obtain structural information about stem I and the stem I – ligand binding loop interface.

Determination of optimal solution conditions

Both sequences fold readily into monomeric hairpin structures and form dye – RNA complexes upon addition of TMR or MG. A varying degree of structural heterogeneity, as assessed by 1D NMR spectroscopy in 90% H_2O, was observed depending on pH and salt concentrations. A wide variety of conditions were tested with samples containing 0.1 mM RNA and a twofold excess of dye to find an optimal buffer system for structural studies. For both complexes the best spectra were obtained in 10 mM potassium phosphate buffer, 10 mM KCl at pH 5.8 over a temperature range from 274 – 298 K. All NMR spectra used in this study were acquired under these conditions for the free RNAs and their complexes with MG and TMR.

Comparison of NMR spectra of the TMR and MG complexes

In order to use information from the crystal structure in the determination of the solution structure of the MG – RNA complex it was necessary to establish that both complexes retain the overall conformation that was observed in the crystal. For this purpose NOESY spectra of the TMR – RNA complex were analyzed along with information from the X-ray structure (PDB ID 1F1T). The dye in this structure is intercalated between two G·C base pairs, namely, G8·C28 and G29·C7; the latter is part of the base quadruple. In addition to NOEs to these bases one would expect short distances to protons in the bases of G24 and A31. We assigned all protons that are part of the TMR spin system by using 2D NMR spectra (DQF COSY, CITY-TOCSY, and NOESY) acquired in 100% D_2O. This process was straightforward owing to the fact that there is little overlap between RNA and dye signals. By using these assignments as a starting point, RNA base protons in the vicinity of the dye were identified by using NOESY spectra and classified by base type from $^1H/^{13}C$ correlation spectra. A comparison of the number and patterns of observed NOEs with those expected based on the X-ray structure clearly indicated that the overall stacking arrangement remains the same in solution and the crystal (with the exception of the A9/A30 stacking which seems to be absent in the TMR complex in solution). Next we had to establish that the TMR and the MG – RNA complexes were sufficiently similar. This was achieved by using a qualitative comparison of NOESY spectra from both complexes. Overlays of NOESY spectra acquired in H_2O and D_2O show many similarities in chemical shifts and NOE patterns observed for nucleotides that have NOEs to the bound ligand (data not shown). Based on these observations we concluded that the binding pockets for the two dyes are similar and thus the X-ray structure can provide useful information for the assignment of the MG – RNA complex spectra.

Resonance assignments in MG – RNA complex

Resonance assignments were based on NMR spectra that were acquired by using four samples: an unlabeled complex of MG with RNA2, an unlabeled complex of MG and RNA1, a complex of unlabeled RNA1 and ^{13}C-methyl-labeled MG,[42] and a complex containing uniformly $^{13}C/^{15}N$-labeled RNA1. Initially the stem regions were assigned by using 2D NOESY spectra assisted by $^1H/^{13}C$ and $^1H/^{15}N$ correlation spectra following standard procedures.[43–45] The characteristic NOESY patterns of the first G·C base pair and the tetraloops were used as starting points. For the assignment of nucleotides in the internal loop region we adopted an "inside – out" approach: nucleotides in the vicinity of the bound dye were identified by means of NOEs between dye and RNA protons. Next, the spin systems (base protons, H1′, and, where possible, H2′) were completed by using 2D TOCSY and COSY spectra and assigned by base type with the help of heteronuclear correlation spectra. Tentative sequence specific assignments were then obtained by comparing the pattern of NOEs and the type of nucleotide with the X-ray structure of the TMR – RNA complex. By using this approach resonances belonging to five nucleotides in the binding pocket were unambiguously assigned. With these positions as starting points the remaining nucleotides were easily assigned by means of NOE patterns. This approach provided complete assignments of base protons (including imino and amino hydrogens involved in hydrogen bonds), H1′, and H2′.

In order to confirm these results and to obtain a better defined structure for the binding pocket we checked and expanded the resonance assignments by using a more conventional approach. Exchangeable proton resonances were assigned by using a 150-ms mixing time 2D NOESY spectrum acquired in H_2O/D_2O (9:1). Resonance assignments were confirmed by using a $^1H/^{15}N$ HMQC spectrum, which allowed identification of base type (guanine versus uracil) by means of the ^{15}N chemical shift and through-bond correlations between exchangeable and nonexchangeable base protons. We were able to unambiguously assign all imino proton resonances in the molecule and many of the amino resonances in the binding pocket. Nonexchangeable proton resonances were assigned by using a combination of homo- and heteronuclear experiments.[44, 46–50] In addition to the abovementioned homonuclear 2D spectra a 3D NOESY – HMQC experiment was used to analyze heavily overlapped regions. Ribose ^1H and ^{13}C resonances were assigned by using a 3D HCCH – COSY experiment[48, 51, 52] and connected to the corresponding base by through-bond HCN and HCNCH correlations.[53–56] By using this strategy we were able to expand the assignments for the nucleotides in the binding pocket (6 – 11 and 22 – 33) to about 89% of the nonexchangeable protons.

Comparison of free and bound RNA

Changes observed in the NMR spectra of the RNA upon addition of ligand indicate that the RNA adopts a new, more compact fold in its ligand bound form. 1D ^1H NMR spectra acquired in H_2O show that several new imino proton signals appear upon addition of MG. This indicates the formation of stable hydrogen bonds in the ligand binding core of the molecule. Some existing resonances adopt a narrower line shape. In addition, a greatly increased number of NOEs can be observed and assigned in the spectra of the complex (Figure 2 and 3). In the ligand free molecule there is evidence for only one of the base pairs in the internal loop region/binding pocket, that is, the U11·A22 pair. This pair, which in the complex becomes part of the first base triple, is preformed. The formation of the base triples upon addition of ligand can be seen in the spectra acquired in 90% H_2O. For example, the second base triple (C10·G23·A27) is indicated by the shifted and split G23 amino signal and NOEs to A27H2. These observations are consistent with ligand-induced folding of the RNA aptamer in the presence of MG (adaptive binding).

Structure calculations

The NMR spectra of the RNA1 – MG complex were used to extract NOE information as a basis for the calculation of a solution structure. Emphasis was placed on the internal loop region (nucleotides 7 – 11 and 22 – 30) and the tetraloop. This resulted in a total of 423 NOEs, 310 of which involved protons within the

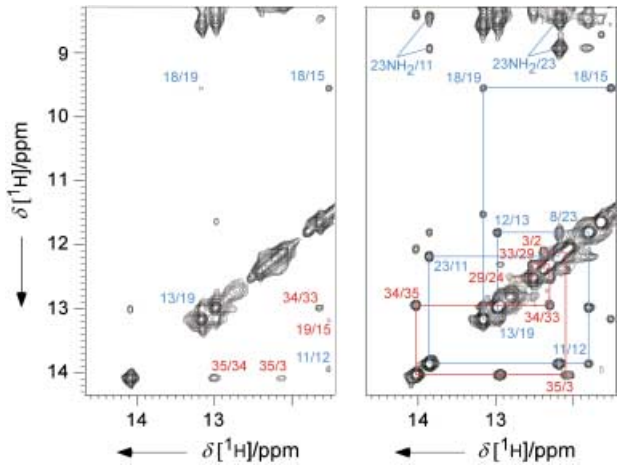

Figure 2. *Imino proton regions of 2D NOESY spectra acquired in 90% H_2O before (left) and after addition of MG (right); 1.0 mM RNA in 10 mM potassium phosphate buffer, 10 mM KCl at pH 5.8. Water suppression was achieved by using the 1̄1-echo sequence. NOESY mixing time was 150 ms. Signals originating from bases in the first stem are labeled in red and for the second stem in blue.*

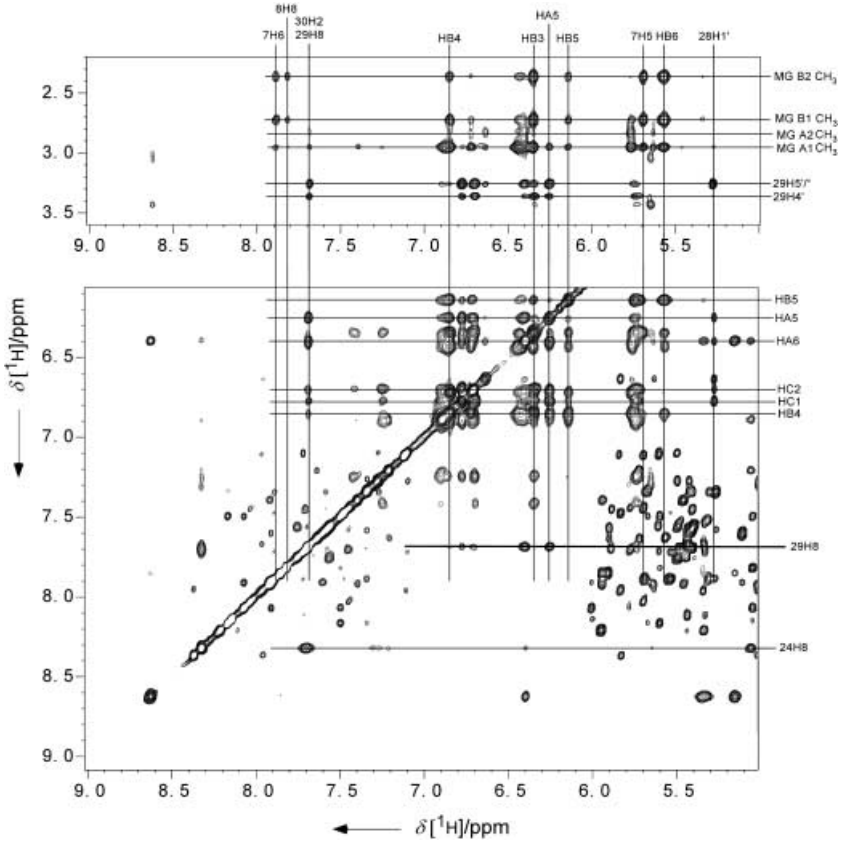

Figure 3. *Two sections of the 2D NOESY of a MG – RNA complex (1:1) acquired in D_2O. The resonance frequencies of protons from several key nucleotides and the bound ligand are labeled. The resonance of MG A1 CH_3 is overlapped with a ribose H2′ resonance.*

internal loop region, 18 involved protons in the tetraloop, and 90 were intermolecular NOEs between RNA and MG (Figure 3). These NOEs were converted into inter-proton distances by using a semiquantitative scale with the H5 – H6 crosspeak intensities of U and C as reference. In addition to these distance restraints the COSY spectra were used to sort the sugar pucker of the riboses into three groups (N type, S type, and unrestrained). The dihedral angle about the glycosidic bond was restrained to the *syn* or *anti* range based on NOE information. These NMR-based restraints were supplemented with hydrogen bond and weak planarity restraints for Watson – Crick-type base pairs and dihedral-angle-based restraints to model the A-form portions of the structure. Based on the fact that a qualitative comparison of the NMR data has shown that the overall fold of the MG complex resembles that of the TMR complex determined by X-ray crystallography, we decided to calculate the structure of the new complex by "docking" the new ligand (MG) into a starting structure generated by deleting TMR from the crystal structure and placing MG at a random position at a distance of 20 Å from the RNA. These starting structures were then subjected to a standard simulated annealing protocol.

The above strategy can potentially lead to a strong bias towards the starting structure. To test if this was the case for our system, a second set of structures was calculated. For the latter set, a random extended structure was used as starting structure and subjected to the same calculation protocol as the original set. As expected, the resulting set of structures has a much lower convergence rate (5% of the structures reach low energies) with many structures "trapped" in various impossible conformations. However, the converged structures have energies similar to the 100 final structures (3000 – 4000 kcal mol^{-1}). A comparison of the two sets of structures shows that they are nearly identical, that is, the root-mean-square deviation (RMSD) between structures from different sets is of the same magnitude or smaller than for each of the sets. In summary this indicates that the observed structure is dominated by the NMR data and independent of the starting structure.

By using the approach described above a set of 100 final structures was generated (Table 1). All 100 structures converged to give reasonable residual energies and were used in the analysis below.

Overall structure

The resulting family of 100 final structures is well defined with an RMSD for all heavy atoms of 1.09 Å and of 0.93 Å for the nucleotides in the binding pocket (C6 – U11, A22 – G33, Figure 4). The structures show that the aptamer folds into a stem – loop structure with the internal loop nucleotides tightly packed to form a binding pocket for the dye. The ligand is stacked between the G8·C28 base pair and the base quadruple formed by the C7·G29 Watson – Crick base pair together with G24 and A31. On the

Table 1. NMR and refinement statistics for the family of final structures.

NMR-derived distance and dihedral angle restraints		
	Total	Binding pocket (7 – 11, 22 – 31, MG)
NOE constraints	423	310
Intranucleotide	148	119
Sequential	119	44
Medium to long-range	66	57
RNA – ligand	90	90
Dihedral angle		
From *J*-coupling data	72	7
From A-form modeling	147	N/A
Total experimental restraints	495	317
NOE-derived restraints per residue	10.8	19.4
Structure statistics for the 100 final structures		
NOE violations > 0.5 Å per structure	0	
Average residual NOE violation [Å]	0.126	
Dihedral violations > 10° per structure	0	
Average dihedral angle violation [°]	4.69	
Mean deviation from ideal covalent geometry		
Bond lengths [Å]	0.0049	
Bond angles [°]	1.66	
Impropers [°]	1.391	
Average pairwise RMSD [Å] for all heavy atoms of the 100 final structures		
All residues	1.09	
Internal loop (6 – 11,22 – 33)	0.93	
GNRA loop (14 – 19)	0.88	

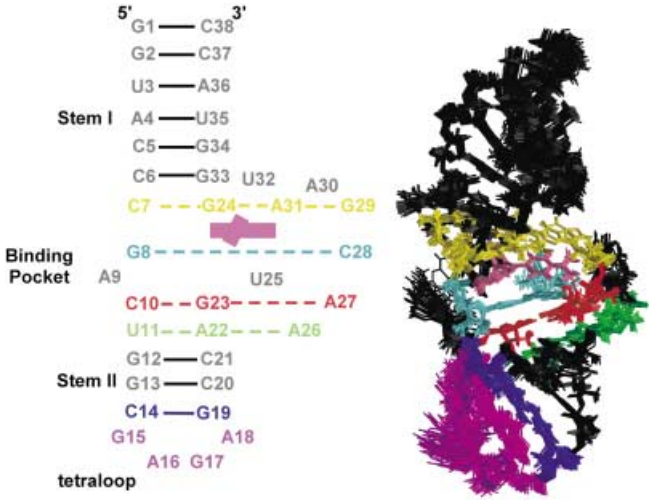

Figure 4. *Base stacking and secondary structure of the MG – RNA complex (left) and overview of the family of the 25 lowest energy final structures (right). Color-coding according to Figure 1. The structures were fitted to the heavy atoms of nucleotides 6 – 10 and 23 – 33 by using MOLMOL.[80]*

stem I side the base quadruple is stacked onto the C6 · G33 pair, and on the stem II side the binding pocket is capped by two base triples, C10 · G23 · A27 and U11 · A22 · A26. Two nucleotides in the base triples, A26 and A27, are also part of a U-turn motif that includes U25 and C28. The turn stabilizes the binding pocket by connecting three of its structural elements, the two base triples and the G8 · C28 base pair.

Structural details and comparison to the crystal structure

The GAGA tetraloop

The GNRA-type tetraloop of the molecule adopts a non-native fold in the X-ray structure as a result of crystal contacts (see below). The four bases are arranged in a 2 – 2 stack rather than the 1 – 3 stacking arrangement commonly observed in solution structures.[57, 58] In all 100 final structures the tetraloop adopts the standard fold originally observed in the solution structure of the GAGA tetraloop from Jucker et al.[57] (PDB ID 1ZIG) with the base of A16 stacked on top of G17 (Figure 5). The turn of the backbone is located between G15 and A16. This is in sharp contrast to the X-ray structure in which the backbone turn occurs between A16 and G17 and the base of A16 is rotated by 180° relative to its position in the solution structure (Figure 5).

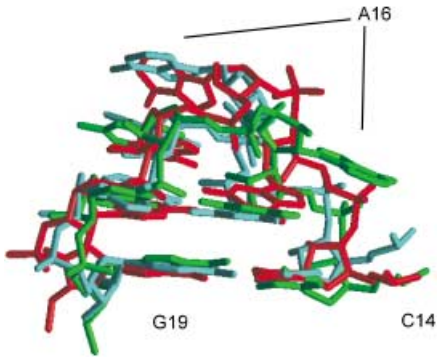

Figure 5. *Superposition of the GNRA tetraloop region (C14 – G19) of the X-ray structure (green, from 1F1T), the solution structure of an isolated GAGA tetraloop (cyan, from 1ZIG), and the lowest energy structure calculated by using NMR restraints (shown in red).*

The base quadruple

The quadruple formed by nucleotides C7, G24, G29, and A31 provides the base of the binding pocket and a stacking platform for the dye. The quadruple can be seen as a combination of a conventional adenosine minor groove triple (essentially identical to the (G23 · C10) · A27 triple described below) and a guanosine major groove triple arranged around a common Watson – Crick base pair between C7 and G29. A31 is hydrogen bonded to G29 through a 6-amino – N3 hydrogen bond and G24 to G29 through 2-amino – O6 and imino – N7 hydrogen bonds. The orientation of the bases and the pattern of hydrogen bonds is very similar in the X-ray structure of the RNA – TMR complex[24] and the solution structure presented here (Figure 6 A). However, the 5′-tail of G24 leads off into the opposite direction in the two structures indicating a different arrangement of the top and bottom of the binding pocket between the two structures. This difference is related to the orientation of U25 discussed below.

The base triples

The two base triples form the top of the binding pocket and do not interact directly with the bound ligand. Nucleotides C10,

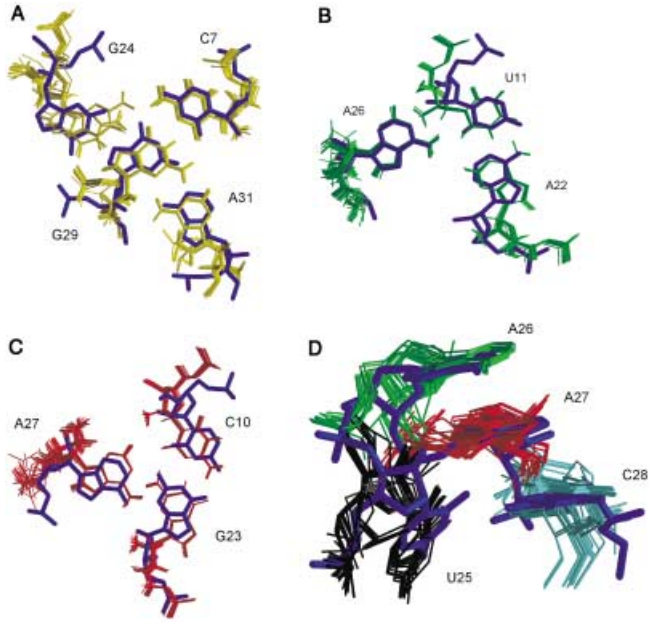

Figure 6. *Detailed comparison of structural motifs in the X-ray structure of the TMR – RNA complex (thick blue bonds) and the solution structure of the MG – RNA complex (25 lowest energy structures, thin bonds, color-coded according to Figure 1). The best fit of the base quadruple (A), the two base triples (B, C), and the U-turn motif (D) are shown.*

G23, and A27 form the inner minor groove (G·C)·A triple which is stacked on top of the G8·C28 base pair. A27 is located in the minor groove of stem II and hydrogen bonds to the Watson – Crick base pair formed by C10 and G23 through a 6-amino – N3 hydrogen bond (Figure 6C). The outer minor groove triple consists of nucleotides U11, A22, and A26. U11 and A22 form a Watson – Crick pair with A26 docked into the minor groove and hydrogen bonded to U11 through a 6-amino – O2 hydrogen bond (Figure 6B). Both base triples are essentially identical in the two structures.

The U-turn motif

The nucleotides U25, A26, A27, and C28 form a tight turn that includes a U-turn motif that closely resembles the one found originally in the anticodon and T-loop of transfer RNA.[59] The phosphate backbone turns after U25. The bases following the turn (A26, A27, C28) are stacked and have their Watson – Crick faces positioned for participating in the base triples and the C28·G8 base pair (Figure 6D). This structure stabilizes and positions several integral parts of the aptamer architecture. A26 and A27 are part of the base triples, C28 is base paired to G8 and stacks on top of the bound dye. The U-turn positions U25 so that it effectively closes the side of the binding pocket and also indirectly stabilizes G24 which stacks below the bound ligand by positioning it such that it can participate in the base quadruple. In both structures U25 is stacked against the *N*-methyl groups of the A ring of the bound dye. However, in the solution structure the position of U25 is not very well defined compared to other parts of the internal loop. This is consistent with an increased mobility of the base in the complex as indicated by the relaxation behavior. The T_2 measured for the C6 of U25 is by far the longest in the molecule (36.1 ms versus an average of 25.0 ms for all C6 atoms in the molecule). Together these facts indicate that in solution U25 is a flexible element within the RNA structure. The nucleotide can act as a hinge that allows the aptamer to adapt its structure to bind different dyes without disrupting core stacking or hydrogen-bonding patterns within the RNA (discussed below).

Stacking and orientation of the dye

The overall orientations of bound MG and TMR complexed with the aptamer are very similar. Both are intercalated between the G8·C28 base pair and the base quadruple (Figure 7). The stacking interactions with the base quadruple are nearly identical in the two structures with the dye A ring located above G24, the B ring stacked on top of the G29·C7 pair, and the C ring located above G29 pointing towards A31. However, there are significant differences in the orientation of the dyes with respect to the G8·C28 base pair. TMR is stacked almost perfectly with the A and B rings located under C28 and G8, respectively, whereas MG has reduced stacking interactions between its B ring and G8. This is indicated in the NOESY spectra by significant differences in the NOE peak patterns. Whereas the B-methyl protons of TMR show weak NOEs to the G8 ribose protons and strong NOEs to the H8 of G8, this pattern is reversed in the NOESY spectra of the MG – RNA complex. The reason for the observed differences are the different shapes of the two dyes in combination with the conformational changes detected in MG upon binding to the RNA.[11] The A and B rings in TMR are perfectly planar; however, the two rings are rotated relative to each other by approximately 49° in free MG and by 57° in the RNA-bound form. The different ligand structures make it impossible to accommodate favorable stacking interactions for both dyes in the same structural framework. This is compensated in the MG – RNA complex by a rotation of the G8·C28 base pair relative to the base quadruple. This movement is made possible by two flexible elements in the RNA structure. U25 (discussed above) and A9 (see below) act as hinge nucleotides to allow optimal positioning of the two parts of the binding pocket to accommodate planar or nonplanar ligands. The less favorable stacking interactions between dye and RNA resulting for MG, specifically the loss of stacking interactions on one side of the B ring, contribute to the reduced stability of the MG – RNA complex ($K_D = 800$ nM versus 50 nM for the TMR complex). The stacking arrangement in the MG – RNA complex is also in agreement with the observation that the B ring of MG rotates approximately 60° out of plane relative to the A and C rings due to the conformational changes caused by the RNA electrostatic field.[11]

Position of A9 and A30

In the crystal structure of the TMR – RNA complex, A9 and A30 are stacked on each other and A30 is stacked against the C ring of TMR. This interaction connects both strands of the binding pocket and leads to a very compact structure (Figure 7D). The

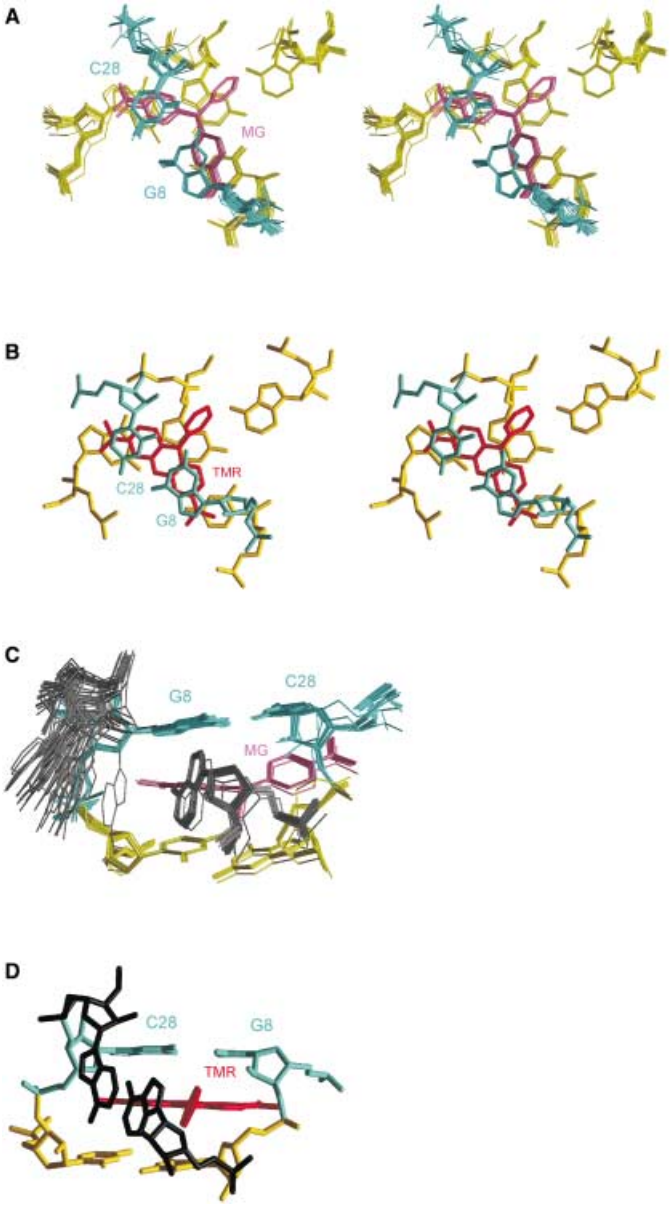

Figure 7. *Comparison of the stacking of MG (A, C) and TMR (B, D) in the aptamer complexes in a top-down stereoview (A, B) and side view of the dye – RNA complexes (C, D). The 25 lowest energy solution structures are shown. Color-coding from Figure 1.*

stacking of the dye C ring with A30 is also found in the MG – RNA complex. NOE connectivities between the H2 of A30 and all protons on the C ring of MG as well as H5 on the B ring place the base in a similar position to that observed in the crystal structure. The same pattern is observed in NOESY spectra of the TMR – RNA complex. However, no NOEs that place A9 anywhere close to A30 were observed under any conditions in either the MG – RNA or the TMR – RNA complex. In the solution structure the position of A9 is not very well defined, but the base is found consistently looped out of the binding pocket (Figure 7C). In fact, a test calculation with artificial NOEs that would place A9 stacked on top of A30 as seen in the crystal structure showed that this arrangement is not consistent with the solution structure and results in NOE violations and increased energies of the final structures (data not shown).

The differences between the two structures with respect to the position of A9 are at least in part related to the different environment, that is, crystal versus solution. In the X-ray structure of the TMR – RNA complex, A30 and A9 from one molecule form a continuous stack with the corresponding bases from a second molecule in the unit cell (Figure 8, top). This

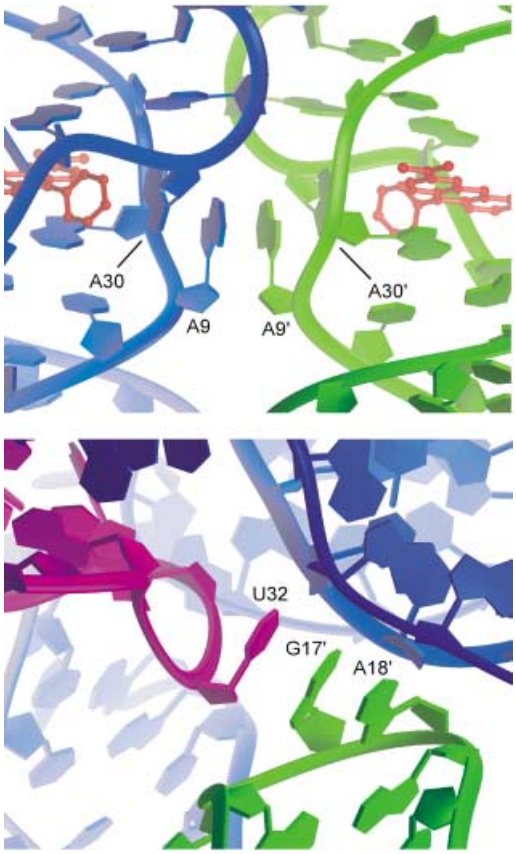

Figure 8. *Crystal contacts in the TMR – RNA complex involving bases in the GNRA tetraloop (bottom) and the A30, A9 stack (top). The different molecules in the unit cell are shown in green, blue, and cyan.*

interaction is similar to the intermolecular stacking that causes the noncanonical structure of the GNRA tetraloop discussed above, with A16 and G17 of one molecule stacking with U32 from a second molecule (Figure 8, bottom). In solution these additional contacts are absent and the conformation observed in the crystal becomes less stable. The inability of the MG – RNA complex to engage in the favorable intermolecular stacking arrangement of A9 and A30 might also contribute to the difficulties in obtaining usable crystals for this aptamer complex.

RNA mutants and stability of the binding pocket

In order to explore how the different structural components contribute to the overall stability of the complex, key nucleotides in the binding pocket were mutated and the dissociation constants of the TMR – RNA complexes were measured (Table 2).

Table 2. *Binding data for RNA mutants of the malachite green binding aptamer in complex with TMR.*

Wildtype	Mutant	Dissociation constant (K_D)	$\Delta\Delta G$ [kcal][a]
U-turn			
U25	C25	368 nM	− 1.18
U25	G25	1.9 μM	− 2.15
U25	A25	≈ 5 – 6 μM	− 2.84
A9/A30 stack			
A9	C9	2.9 μM	− 2.41
A9	G9	64 nM	− 0.15
A9	U9	140 nM	− 0.61
A30	G30	1.6 μM	− 2.05
A30	C30	500 nM	− 1.36
A30	U30	4.6 μM	− 2.68
Base triple 1			
A27	C27	4.01 μM	− 2.60
A27	G27	≈ 6 – 7 μM	− 2.93
A27	U27	≈ 7 – 8 μM	− 3.00
C10G23	G10C23	338 nM	− 1.14
Base triple 2			
A26	G26	≈ 8 – 9 μM	− 3.01
A26	U26	≈ 4 – 5 μM	− 2.72
A26	C26	6 μM	− 2.48
U11A22	A11U22	48 nM	+ 0.024
Base quadruple			
G24	C24	512 nM	− 1.38
A31	G31	7.2 μM	− 2.95
A31	C31	1.2 μM	− 1.88
A31	U31	1.95 μM	− 2.17
G8/C28 base pair			
G8C28	C8G28	≈ 5 – 6 μM	− 2.83

[a] The difference between the free energies of binding of wildtype (K_D = 50 nM) and mutant RNA – TMR complexes was calculated as $\Delta\Delta G = RT(\ln K_{D,WT} - \ln K_{D,Mut})$ at 293 K.

The K_D values for the mutant complexes and the change in the free energy of binding ($\Delta\Delta G$) compared to the wildtype complex indicate the relative importance of the various structural features for the integrity of the binding pocket. For example, the U-turn motif is very sensitive to mutations. Introduction of a purine in the position of U25 leads to a 38-fold and a more than 100-fold increase of K_D for G and A, respectively. A cytosine is slightly better tolerated with only a sevenfold increase of K_D indicating that the size of the base in this position is a crucial factor.

The A9/A30 stack observed in the crystal structure does not seem to be present in solution for both the TMR and the MG – RNA complex. This would suggest that mutations of A9 (the "outer" A) should have only a very minor effect on complex stability because the base is highly mobile in solution and does not seem to have any permanent interactions with other parts of the binding pocket or the ligand. Indeed, A9 can be mutated to a G or U with only a less than threefold increase of K_D. The very large K_D value for the A9/C9 exchange does not fit this pattern and is most likely an artifact owing to formation of an alternative structure that interferes with folding (i.e., an alternative base pairing scheme). A30 substitutions are much less well tolerated and lead to at least a tenfold increase of the complex dissociation constant. Both base triples are crucial for complex stability even though they do not interact directly with the ligand. Any substitution of the third strand adenines (A26 and A27) results in an 80-fold or larger increase of the complex K_D values. In contrast, a flip of the central Watson – Crick base pairs is fairly well tolerated with no change of K_D for triple 2 and only a 6.8-fold increase for triple 1. This indicates that the main function of the base triples is to position and stabilize the U-turn nucleotides that shape the top of the binding pocket. The base quadruple and the G8·C28 base pair form the stacking platforms for the ligand and are very sensitive to mutations as would be expected. The very large effect of the G8·C28 base pair flip indicates that optimal stacking interactions between ligand and RNA are crucial for complex stability. A comparison of stacking interactions in the structures of the TMR and MG – RNA complexes (Figure 7) and the corresponding complex dissociation constants allows one to qualitatively assess the magnitude of the base – ligand stacking interactions. The nonplanar arrangement of the rings in MG clearly reduces all favorable stacking interactions somewhat. However, the single largest change results from the complete loss of interactions between ring B of MG and guanine 8. Together these changes in the stacking are responsible for a 16-fold increase of the dissociation constant of the MG complex relative to the TMR complex.

Ligand binding and charge distribution in the binding pocket

A comparison of binding data for several derivatives of MG shows that the aptamer can accommodate a variety of molecules in its binding pocket.[24] TMR has the lowest complex dissociation constant of all tested dyes (K_D = 50 nM). Pyronin Y, essentially a TMR molecule without the C-phenyl ring, binds with a K_D of 225 nM, and MG has an even lower affinity with a K_D of 800 nM. Crystal violet (CV), an MG derivative with an additional *N*-dimethyl group located in the *para* position on ring C, has a K_D value larger than 1 mM. This very high K_D value is surprising and cannot easily be explained by disruption of stacking interactions or steric clashes. Modeling studies based on the two complex structures and free CV indicate that the ligand "should" fit into the binding pocket. A closer look at the ligand and its electronic structure point at a major role for electrostatic interactions in ligand binding in this aptamer complex.[42] In CV, the positive charge is equally distributed across all three rings with partial charges of approximately + 0.33 for each ring. The electrostatics of the binding pocket are largely determined by the position of the RNA backbone phosphates. The highest density of close phosphate groups is found in the vicinity of ring A followed closely by ring C (Figure 9). A likely reason for the greatly reduced binding of CV is that CV cannot adapt its charge distribution well enough to compensate for the asymmetry of the binding pocket due to its highly delocalized ("diluted") charge.

Discussion

The mode of binding encountered in most small-molecule – RNA complexes that have been characterized by NMR spectroscopy or X-ray crystallography to date poses a challenge for rational, structure-based drug or ligand design. The ligand-induced

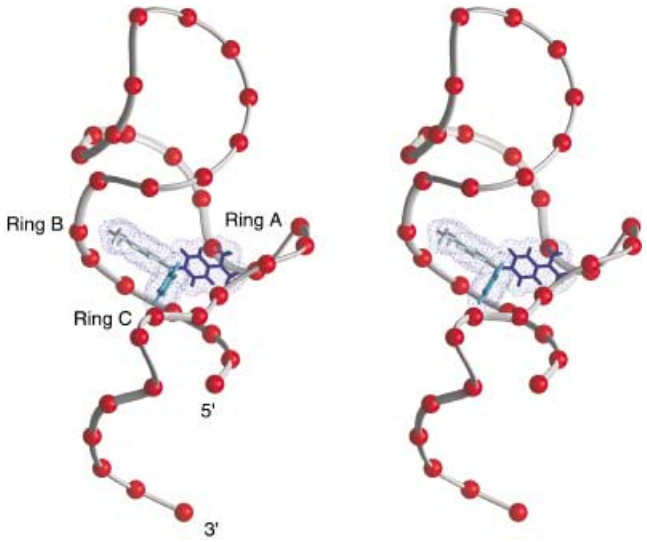

Figure 9. *Stereoview of the malachite green binding aptamer. The RNA backbone is shown as a gray ribbon with the phosphate atoms displayed as red spheres. MG is shown in thick bonds with a transparent van der Waals surface. The coloring for MG indicates relative distribution of the positive charge (darker blue corresponds to larger partial charge).*

folding and structural changes of the RNA that are observed during adaptive binding suggest that traditional docking strategies will fail in many cases due to the difficulty of defining the structure of the target "binding pocket", that is, how the RNA reacts to the presence of a different ligand. This situation is further complicated by the structural changes in the ligand upon complex formation.

The comparison of the X-ray structure of the TMR–RNA complex with the solution structure of the MG–RNA complex presented here provides a glimpse at how the binding pocket of the aptamer can adapt to the structures of planar and nonplanar ligands. Rotation of the base pairs above and below the ligand can accommodate dye derivatives with nonplanar ring systems without disrupting any crucial RNA structure elements. The adaptability of the aptamer with respect to the different ligands is largely facilitated by two flexible elements in the RNA structure, A9 and U26. Moreover, the two structures allow a discussion of structural changes that have been observed in the ligand[11] in the context of the overall complex structure. Base pairing and stacking interactions within the RNA fold the phosphate backbone into a structure that results in an asymmetric charge distribution within the binding pocket that forces the ligand to adapt through the redistribution of the positive partial charge (Figure 9).

Experimental Section

RNA sample preparation: Samples of the malachite green binding aptamer were prepared enzymatically from a synthetic DNA template by using T7 RNA polymerase[60] and unlabeled or $^{13}C/^{15}N$-labeled NTPs[61] as previously described.[9, 62] To reduce nontemplated nucleotide addition at the 3′-end of the transcribed RNA, the DNA templates were synthesized to have the last two (5′) nucleotides replaced with their 2′-methoxy analogues[63] (Oligos Etc. Inc., Wilsonville, OR). NMR samples for use in studying exchangeable protons were prepared by dissolving the lyophilized RNA in a H_2O/D_2O (9:1) solution and adjusting to pH 5.8 with NaOH (unless otherwise stated). Samples used for studying nonexchangeable protons were prepared by dissolving the RNA in 99.996% D_2O (Isotec). All NMR samples were 500 μL in standard 5-mm NMR tubes with final RNA concentrations of 0.8–1.8 mM in 10 mM potassium phosphate buffer (pH 5.8) and 10 mM KCl.

NMR spectroscopy: All spectra were collected on a Bruker DRX-600 spectrometer equipped with a HCN triple resonance, triple-axis PFG probe. Solvent suppression for samples in H_2O/D_2O (9:1) was achieved by using 1$\bar{1}$-spin echo pulse sequences[64] or WATERGATE.[65] Quadrature detection for the indirect dimensions in multidimensional experiments was achieved by using the States-TPPI method.[66] 2D NOESY spectra[67] in H_2O/D_2O (9:1) were acquired at 274 K and 283 K with a mixing time of 150 ms. A 2D CITY–TOCSY[68] with a mixing time of 50 ms, a DQF–COSY,[69] and NOESY spectra with mixing times of 250, 200, and 50 ms in 100% D_2O were measured at 298 K.

Heteronuclear experiments were acquired at 293 K in 100% D_2O, with the exception of a $^1H/^{15}N$ HMQC and an HCCNH–TOCSY[70] which were acquired in H_2O/D_2O (9:1) at 274 K. Broadband decoupling for ^{13}C and ^{15}N during acquisition was achieved by using the GARP[71] composite pulse sequence. 2D spectra acquired included $^{15}N/^1H$ and $^{13}C/^1H$ HSQC,[72] $^{15}N/^1H$ long-range HSQC[73] spectra, and an HCNCH experiment.[55] A 3D $^{13}C/^1H$ NOESY–HMQC[74] (mixing time 200 ms) and a 3D HCCH–COSY[75] were used to resolve overlaps and assign ribose resonances. T_2 values were determined by using an HSQC pulse sequence with added relaxation delays as described previously.[76] All spectra were processed by using the XWIN-NMR 2.6 software package (Bruker Inc.) and analyzed by using XEasy[77] on a Silicon Graphics O2 workstation. ^1H chemical shifts were referenced to an external standard of DSS, and ^{13}C and ^{15}N chemical shifts were calculated indirectly as recommended by Markley et al.[78]

NOE distance and dihedral angle constraints: Nonexchangeable inter-proton restraints were obtained from NOESY spectra of samples in D_2O acquired at 293 K with 250-, 200-, and 50-ms mixing times as well as the three-dimensional $^{13}C/^1H$ NOESY–HMQC. NOE distances involving exchangeable proton resonances were obtained from a 2D NOESY in H_2O/D_2O (9:1) at 274 K with a 150-ms mixing time. NOE distances for nonexchangeable protons were obtained by integrating crosspeak volumes and by using the R^{-6} relationship between intensity and distance. For calibration, we used the average pyrimidine H5–H6 crosspeak volume as a standard reference of 2.4 Å. An additional 0.8 Å was added to each distance for the upper bounds, while lower bounds were set equal to the sum of the van der Waals radii. Dihedral angle restraints for the ribose sugar puckers were obtained from analysis of DQF–COSY spectra. Residues that gave H1′–H2′ coupling constants larger than approximately 9 Hz were restrained to an S-type range ($v_1 = 21 \pm 5^\circ$ and $v_2 = -36 \pm 5^\circ$). Residues with intermediate coupling constants ($\approx$4–7 Hz) were left unrestrained. The residues with small or absent H1′–H2′ crosspeaks were restrained to an N-type range ($v_1 = -22 \pm 5^\circ$ and $v_2 = 36 \pm 5^\circ$).

Structure calculations: All structure calculations were done with CNS v1.1.[79] The two A-form-like stem regions were modeled as A-form RNA by using artificial hydrogen bond and dihedral restraints in combination with the NOE data. Hydrogen bond restraints (two per hydrogen bond) were included for those Watson–Crick base pairs that displayed slowly exchanging imino protons and NOEs

indicative of base pairing. Structure calculations were started from a model structure generated based on the crystal structure (PDB ID 1F1T) to which protons were added. The TMR ligand in this structure was deleted and a minimized structure of MG was placed at a distance of 20 Å in a random orientation. These structures were then subjected to a simulated annealing protocol for 20 ps at 1000 K with 1-fs time steps, followed by a cooling phase (20 ps of cooling from 1000 K to 0 K with 1-fs time steps). This was then followed by 2000 minimization steps. The NOE scale factor was set to 150 for all parts of the calculations except in the minimization steps for which it was set to 75. The 100 final structures were used for detailed analysis by using the software packages MOLMOL[80] and WebLab Viewer Pro (Molecular Simulations Inc.). Hydrogen bonds were analyzed with MOLMOL by using criteria in which the angle between proton donor and acceptor must be greater than 120° and the distance less than 2.5 Å.

Coordinates: Atomic coordinates for the 10 lowest energy structures have been deposited in the RCSB Protein Data Bank (accession number 1Q8N).

Measurement of binding affinities: Binding of the fluorophore TMR to the aptamer was measured by monitoring changes in fluorescence intensity or anisotropy with a Perkin – Elmer LS50B Luminescence Spectrometer as described previously.[24]

Acknowledgements

The authors thank Dr. Dara Gilbert for helpful discussions and Ms. Janet Trang for technical assistance. This work was supported by NSF grant MCB0110689 to T.D.. The 600 MHz NMR spectrometer was purchased with funds from NIH grant RR11973. J.F. acknowledges support by the University of California Systemwide Biotechnology Program (Grant No. 2001 – 7).

Keywords: electrostatic interactions · ligand – RNA interactions · NMR spectroscopy · RNA structures · stacking interactions

[1] R. Schroeder, C. Waldsich, H. Wank, *EMBO J.* **2000**, *19*, 1.
[2] Q. Chen, R. H. Shafer, I. D. Kuntz, *Biochemistry* **1997**, *36*, 11 402.
[3] T. Hermann, E. Westhof, *J. Med. Chem.* **1999**, *42*, 1250.
[4] A. V. Filikov, V. Mohan, T. A. Vickers, R. H. Griffey, P. D. Cook, R. A. Abagyan, T. L. James, *J. Comput.-Aided Mol. Des.* **2000**, *14*, 593.
[5] K. E. Lind, Z. H. Du, K. Fujinaga, B. M. Peterlin, T. L. James, *Chem. Biol.* **2002**, *9*, 185.
[6] T. Dieckmann, S. E. Butcher, M. Sassanfar, J. W. Szostak, J. Feigon, *J. Mol. Biol.* **1997**, *273*, 467.
[7] D. J. Patel, A. K. Suri, F. Jiang, L. Jiang, P. Fan, R. A. Kumar, S. Nonin, *J. Mol. Biol.* **1997**, *272*, 645.
[8] J. R. Williamson, *Nat. Struct. Biol.* **2000**, *7*, 834.
[9] T. Dieckmann, E. Suzuki, G. K. Nakamura, J. Feigon, *RNA* **1996**, *2*, 628.
[10] F. Jiang, R. A. Kumar, R. A. Jones, D. J. Patel, *Nature* **1996**, *382*, 183.
[11] D. Nguyen, S. C. DeFina, W. Fink, T. Dieckmann, *J. Am. Chem. Soc.* **2002**, *124*, 15 081.
[12] A. D. Ellington, J. W. Szostak, *Nature* **1990**, *346*, 818.
[13] C. Tuerk, L. Gold, *Science* **1990**, *249*, 505.
[14] K. W. Uphoff, S. Bell, A. D. Ellington, *Curr. Opin. Struct. Biol.* **1996**, *6*, 281.
[15] H. A. Heus, *Nat. Struct. Biol.* **1997**, *4*, 597.
[16] D. S. Wilson, J. W. Szostak, *Annu. Rev. Biochem.* **1999**, *68*, 611.
[17] R. F. Macaya, P. Schultze, F. W. Smith, J. A. Roe, J. Feigon, *Proc. Natl. Acad. Sci. USA* **1993**, *90*, 3745.
[18] P. Fan, A. K. Suri, R. Fiala, D. Live, D. J. Patel, *J. Mol. Biol.* **1996**, *258*, 480.
[19] Y. Yang, M. Kochoyan, P. Burgstaller, E. Westhof, M. Famulok, *Science* **1996**, *272*, 1343.
[20] J. Feigon, T. Dieckmann, F. W. Smith, *Chem. Biol.* **1996**, *3*, 611.
[21] L. C. Jiang, D. J. Patel, *Nat. Struct. Biol.* **1998**, *5*, 769.
[22] M. A. Convery, S. Rowsell, N. J. Stonehouse, A. D. Ellington, I. Hirao, J. B. Murray, D. S. Peabody, S. E. V. Phillips, P. G. Stockley, *Nat. Struct. Biol.* **1998**, *5*, 133.
[23] G. R. Zimmermann, C. L. Wick, T. P. Shields, R. D. Jenison, A. Pardi, *RNA* **2000**, *6*, 659.
[24] C. Baugh, D. Grate, C. Wilson, *J. Mol. Biol.* **2000**, *301*, 117.
[25] D. Sussman, C. Wilson, *Structure* **2000**, *8*, 719.
[26] D. Sussman, J. C. Nix, C. Wilson, *Nat. Struct. Biol.* **2000**, *7*, 53.
[27] W. C. Winkler, S. Cohen-Chalamish, R. R. Breaker, *Proc. Natl. Acad. Sci. USA* **2002**, *99*, 15 908.
[28] W. Winkler, A. Nahvi, R. R. Breaker, *Nature* **2002**, *419*, 952.
[29] A. Nahvi, N. Sudarsan, M. S. Ebert, X. Zou, K. L. Brown, R. R. Breaker, *Chem. Biol.* **2002**, *9*, 1043.
[30] K. Konopka, N. Duzgunes, J. Rossi, N. S. Lee, *J. Drug Targeting* **1998**, *5*, 247.
[31] X. H. Fang, Z. H. Cao, T. Beck, W. H. Tan, *Anal. Chem.* **2001**, *73*, 5752.
[32] Q. Deng, I. German, D. Buchanan, R. T. Kennedy, *Anal. Chem.* **2001**, *73*, 5415.
[33] M. A. Rehder, L. B. McGown, *Electrophoresis* **2001**, *22*, 3759.
[34] N. Hamaguchi, A. Ellington, M. Stanton, *Anal. Biochem.* **2001**, *294*, 126.
[35] M. N. Stojanovic, P. de Prada, D. W. Landry, *J. Am. Chem. Soc.* **2001**, *123*, 4928.
[36] K. Konopka, N. S. Lee, J. Rossi, N. Duzgunes, *Gene* **2000**, *255*, 235.
[37] O. Kensch, B. A. Connolly, H. J. Steinhoff, A. McGregor, R. S. Goody, T. Restle, *J. Biol. Chem.* **2000**, *275*, 18 271.
[38] G. A. Soukup, R. R. Breaker, *Curr. Opin. Struct. Biol.* **2000**, *10*, 318.
[39] G. A. Soukup, R. R. Breaker, *Trends Biotechnol.* **1999**, *17*, 469.
[40] M. Sassanfar, J. W. Szostak, *Nature* **1993**, *364*, 550.
[41] D. Grate, C. Wilson, *Proc. Natl. Acad. Sci. USA* **1999**, *96*, 6131.
[42] S. C. DeFina, T. Dieckmann, *J. Label Compd Radiopharm* **2002**, *45*, 241.
[43] K. Wüthrich, *NMR of Proteins and Nucleic Acids*, Wiley, New York, **1986**.
[44] T. Dieckmann, J. Feigon, *J. Biomol. NMR* **1997**, *9*, 259.
[45] E. T. Mollova, A. Pardi, *Curr. Opin. Struct. Biol.* **2000**, *10*, 298.
[46] T. Dieckmann, J. Feigon, *Curr. Opin. Struct. Biol.* **1994**, *4*, 745.
[47] E. P. Nikonowicz, A. Pardi, *Nature* **1992**, *355*, 184.
[48] A. Pardi, E. P. Nikonowicz, *J. Am. Chem. Soc.* **1992**, *114*, 9202.
[49] B. T. Farmer, II, L. Muller, E. P. Nikonowicz, A. Pardi, *J. Am. Chem. Soc.* **1993**, *115*, 11 040.
[50] E. P. Nikonowicz, A. Pardi, *J. Mol. Biol.* **1993**, *232*, 1141.
[51] J. P. Marino, J. H. Prestegard, D. M. Crothers, *J. Am. Chem. Soc.* **1994**, *116*, 2205.
[52] H. Wang, E. R. P. Zuiderweg, *J. Biomol. NMR* **1995**, *5*, 207.
[53] V. Sklenář, R. D. Peterson, M. R. Rejante, J. Feigon, *J. Biomol. NMR* **1993**, *3*, 721.
[54] L. Mueller, E. P. Nikonowicz, B. T. Farmer, II, A. Pardi, *J. Biomol. NMR* **1994**, *4*, 129.
[55] V. Sklenář, R. D. Peterson, M. R. Rejante, E. Wang, J. Feigon, *J. Am. Chem. Soc.* **1993**, *115*, 12 181.
[56] V. Sklenář, T. Dieckmann, S. E. Butcher, J. Feigon, *J. Magn. Reson.* **1998**, *130*, 119.
[57] F. M. Jucker, A. Pardi, *RNA* **1995**, *1*, 219.
[58] H. A. Heus, A. Pardi, *Science* **1991**, *253*, 191.
[59] G. J. Quigley, A. Rich, *Science* **1976**, *194*, 796.
[60] J. F. Milligan, D. R. Groebe, G. W. Witherell, O. C. Uhlenbeck, *Nucleic Acids Res.* **1987**, *15*, 8783.
[61] R. T. Batey, J. L. Battiste, J. R. Williamson, in *Methods in Enzymology, Vol. 261* (Ed.: T. L. James), Academic Press, San Diego, **1995**, p. 300.
[62] J. Flinders, T. Dieckmann, *J. Mol. Biol.* **2001**, *308*, 665.
[63] C. Kao, M. Zheng, S. Rudisser, *RNA* **1999**, *5*, 1268.
[64] V. Sklenář, A. Bax, *J. Magn. Reson.* **1987**, *74*, 469.
[65] M. Piotto, V. Saudek, V. Sklenář, *J. Biomol. NMR* **1992**, *2*, 661.
[66] D. Marion, M. Ikura, R. Tschudin, A. Bax, *J. Magn. Reson.* **1989**, *85*, 393.
[67] A. Kumar, R. R. Ernst, K. Wüthrich, *Biochem. Biophys. Res. Comm.* **1980**, *95*, 1.
[68] J. Briand, R. R. Ernst, *Chem. Phys. Let.* **1991**, *185*, 276.
[69] U. Piantini, O. W. Sørensen, R. R. Ernst, *J. Am. Chem. Soc.* **1982**, *104*, 6800.
[70] V. Sklenář, T. Dieckmann, S. E. Butcher, J. Feigon, *J. Biomol. NMR* **1996**, *7*, 83.
[71] A. J. Shaka, P. Barker, R. Freeman, *J. Magn. Reson.* **1985**, *64*, 547.
[72] L. E. Kay, P. Keifer, T. Saarinen, *J. Am. Chem. Soc.* **1992**, *114*, 10 663.

[73] V. Sklenář, R. D. Peterson, M. R. Rejante, J. Feigon, *J. Biomol. NMR* **1994**, *4*, 117.
[74] D. Marion, L. E. Kay, S. W. Sparks, D. A. Torchia, A. Bax, *J. Am. Chem. Soc.* **1989**, *111*, 1515.
[75] L. E. Kay, M. Ikura, A. Bax, *J. Am. Chem. Soc.* **1990**, *112*, 888.
[76] L. E. Kay, D. A. Torchia, A. Bax, *Biochemistry* **1989**, *28*, 8972.
[77] C. Bartels, T. H. Xia, M. Billeter, P. Guntert, K. Wüthrich, *J. Biomol. NMR* **1995**, *6*, 1.
[78] J. L. Markley, A. Bax, Y. Arata, C. W. Hilbers, R. Kaptein, B. D. Sykes, P. E. Wright, K. Wüthrich, *J. Mol. Biol.* **1998**, *280*, 933.
[79] A. T. Brunger, P. D. Adams, G. M. Clore, W. L. DeLano, P. Gros, R. W. GrosseKunstleve, J. S. Jiang, J. Kuszewski, M. Nilges, N. S. Pannu, R. J. Read, L. M. Rice, T. Simonson, G. L. Warren, *Acta Crystallogr., Sect. D: Biol. Crystallogr.* **1998**, *54*, 905.
[80] R. Koradi, M. Billeter, K. Wüthrich, *J. Mol. Graphics* **1996**, *14*, 51 +.

Received: June 25, 2003 [F 701]